Structural relaxation and longitudinal dipole moment of $SrTiO_3(001)(1\times1)$ surfaces

C. Cheng,[1,*] K. Kunc,[2,†] and M. H. Lee[3,‡]
[1]*Department of Physics, National Cheng Kung University, Tainan, Taiwan, Republic of China*
[2]*Laboratoire d'Optique des Solides associé au CNRS, T13 - C80, 4 place Jussieu, 75252 Paris - Cedex 05 France*
[3]*Department of Physics, Tamkang University, Tamsui, Taipei 251, Taiwan, Republic of China*
(Received 5 January 2000)

First-principles calculations are employed to study $SrTiO_3(001)$ (1×1) surfaces with both SrO and TiO_2 termination. A detailed geometry of the relaxed systems, surface energy, and the individual relaxation energies of the two types of surface are obtained. The longitudinal surface dipole moments are derived from variation of the macroscopic electrostatic potential along the surface normal direction. Pseudopotential–plane-wave calculations are performed in the slab geometry, on both symmetric and asymmetric slabs; the merits and the limits of the latter geometry are discussed.

I. INTRODUCTION

The renewed interest in the $SrTiO_3(001)$ surfaces is due to their use as substrate for growing epitaxial films of high-T_c superconductors.[1] In this context questions arise about the surface ferroelectric reconstruction, i.e., structural modifications parallel[2,3] or perpendicular[4–6] to the surface. In contrast to other ABO_3 oxides (e.g., $BaTiO_3$), bulk $SrTiO_3$ remains paraelectric in the cubic perovskite structure (Fig. 1) at finite temperatures down to 105 K.[7] This structure allows two types of (001) termination, viz., the SrO- or the TiO_2-terminated surface (Fig. 1). Both can be realized experimentally by atomically controlled growth.[8] Besides (1×1) surface structures, more complicated reconstructions of the (001) surface have been reported.[9] Since these surface layers consist of both cations and anions, surface reconstruction might generate permanent dipole moments, which raises the question of permanent surface polarization.

In this article, we shall concentrate on the ''longitudinal'' effects caused by the relaxation *perpendicular* to the surface, in particular on the surface dipole moments. Using *ab initio* methods, we find the detailed atomic structure of both the SrO- and TiO_2-terminated $SrTiO_3(001)$ (1×1) surfaces, the surface energy, and the individual relaxation energies for the two types of surfaces. The longitudinal dipole moments (before and after relaxation) are then obtained from the analysis of the macroscopic electrostatic potential and its variation along the direction normal to the surface.

Most previous calculations[2,6,10] relied on model descriptions, e.g., the shell model (better known from lattice dynamics), and the atomic reconstruction and surface energies have recently been addressed[3,4] by first-principles methods similar to those applied here. The present work focuses on surface polarization effects. Nevertheless, in order to ensure the consistency between the electrostatics and the geometry of the surface, we also repeat the determination of the atomic arrangements within our present calculational scheme. In turn, the existence of two sets of results for surface reconstruction, coming from two different *ab initio* calculations, presents then the opportunity to estimate numerical errors and, more generally, to assess the uncertainties of the first-principles determination of atomic geometries. On the technical side, we employ for calculation of surface properties both symmetric and *asymmetric* slabs. As the latter construction has usually been avoided in surface calculations, we discuss the macroscopic fields arising in the asymmetric periodic cells and the precautions that should be observed when using this geometry.

The present paper is organized as follows: The details of the calculations are explained in Sec. II. Section III contains the results of the relaxed structures and Sec. IV the discussion of surface energies. In Sec. V we describe how the longitudinal surface dipole moments are obtained. The particularities of the asymmetric-slab calculations are discussed in Sec. VI.

II. CALCULATION DETAILS

The calculations we perform are based on density functional theory[11] within the local density approximation[12] (LDA) using the Ceperley-Alder form[13] for exchange correlation, employing the *CASTEP* codes[14] (Cambridge Serial Total Energy Package) for performing all the self-consistent calculations. Periodic slabs separated by vacuum are used to simulate the surface systems. The one-electron wave functions are expanded in a plane-wave basis limited by the kinetic energy cutoff $E^{PW}=500$ eV. Integration over the first Brillouin zone uses the discrete *k*-point sampling according

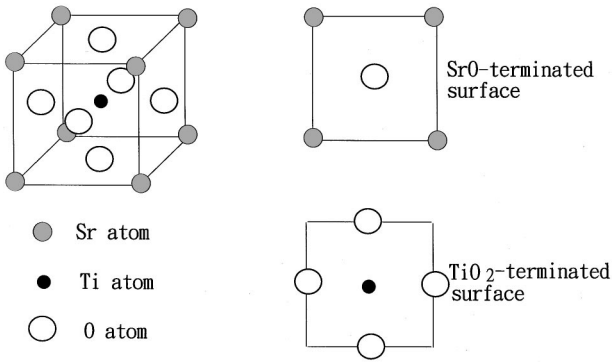

FIG. 1. The cubic perovskite structure of $SrTiO_3$ and the two types of termination of the (1×1) surfaces.

TABLE I. Convergence of the static equilibrium (lattice constant, bulk modulus, and its pressure derivative) of bulk $SrTiO_3$ with respect to energy cutoff E^{pw} and to the Brillouin-zone sampling (number of k points N_k).

N_k	E^{PW}	a_0 (Å)	B_0 (GPa)	B_0'
4	500 eV	3.95	172	3.6
10	500 eV	3.95	174	3.7
4	600 eV	3.93	192	4.9
4	700 eV	3.92	188	4.6
4	800 eV	3.92	191	4.4
Experiment (Ref. 20)		3.9048	183	–

to Monkhost and Pack[15] (see later). The ''optimized'' norm-conserving pseudopotentials[16] in the Kleinman-Bylander representation[17] are used to describe the interactions between valence electrons and ions; the number of valence electrons considered is 10, 4, and 6 for Sr, Ti, and O atoms, respectively. In strontium, the eight semicore electrons from the $4s$ and $4p$ orbitals are treated as valence electrons.[18] The Sr pseudopotential was generated on the $4s^2 4p^6$ configuration, with core radii of 2.5 and 2.2 a.u. for the s and p components, respectively. The Ti pseudopotential was obtained using the $4s^2 3d^2$ configuration for the s and d components and on the $4s^{0.75} 4p^{0.25} 3d^2$ state for p, with the same core radius of 2.5 a.u. for all three components. The O pseudopotential was generated on the $2s^2 2p^4$ state for the s and p and on the $2s^1 2p^{1.75} 3d^{0.25}$ configuration for the d component, with a core radius of 1.4 a.u. for all s, p, and d components. The pseudopotentials are ''optimized''[16] for low plane-wave (PW) cutoffs starting from $E^{PW}=500$ eV. The Ti and O pseudopotentials of this type were already applied in other contexts[19] but that for Sr is used.

In order to check the pseudopotentials and the numerical convergence, we have calculated the equilibrium lattice constant, the bulk modulus, and its pressure derivative for bulk $SrTiO_3$ using increasing numbers of plane waves and k-point sets summarized in Table I. The 4- and 10-k-point sets correspond to the Monkhost-Pack parameters (4 4 4) and (6 6 6). It can be seen that four special k points are sufficient for the Brillouin zone integration. With respect to plane-wave cutoff the static equilibrium results are fully converged at $E^{PW}=600$ eV, but already at $E^{PW}=500$ eV the lattice constant deviates only by about 0.03 Å (0.8%), less than the uncertainty in the experimental data[20] (0.05 Å or 1.3%). Therefore we used a plane-wave cutoff $E^{PW}=500$ eV in all supercell calculations reported here.

To simulate a surface system, we use periodic cells containing seven primitive unit cells of the bulk (Fig. 2). They comprise a slab consisting of 10 or 11 atomic planes of $SrTiO_3$ and vacuum equivalent to another 4 or 5 atomic planes (thickness $2a_0$ or $2.5a_0$). We have checked that this vacuum size is large enough to avoid interaction of one surface with the nearest supercell. In Fig. 2 the slabs (a) and (b) are symmetric with respect to the mirror plane passing through the center of the supercell, whereas the unit cell (c) is *asymmetric* and gives rise to a macroscopic electric field that requires special considerations discussed in Sec. VI.

A convergence test with $E^{PW}=600$ eV shows that both the surface energy and relaxation energies are converged to

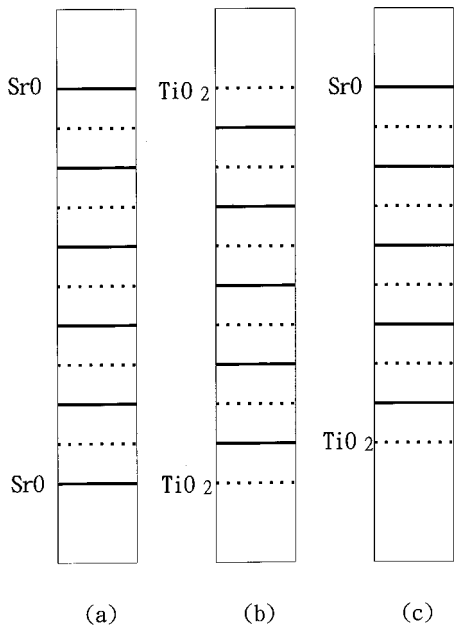

FIG. 2. The translational unit cells used in the present calculations. The slabs in (a) and (b) are symmetric with respect to mirror plane passing through the center of the slab; that in (c) is asymmetric and can give rise to macroscopic field (see Sec. VI). The $+z$ direction, perpendicular to the surfaces, is pointing upwards.

0.01 eV per (1×1) surface area, which represents an uncertainty of 2% and 5%, respectively. The k-point set used in all the supercell calculations is defined[15] by $(q_1 q_2 q_3) = (4\,4\,2)$, which leads to three special k points in the irreducible part of the Brillouin zone. This mesh has the same density in the xy direction as the (4 4 4) mesh used in the bulk calculations. For relaxing atomic positions in the surface structures, we use the forces due to the Hellmann-Feynman theorem[21] to move the atoms to positions at which all forces became smaller than $\delta=0.02$ eV/Å .

III. RELAXED STRUCTURES

The geometry of the relaxed SrO- and TiO_2-terminated surfaces, as calculated for symmetric slabs [Figs. 2(a) and 2(b)], are listed in Table II. The results we obtained on the asymmetric slab according to Fig. 2(c) (not listed) are nearly identical (within 0.01 Å) and their significance will be discussed in Sec. VI.

In Table II the $+z$ direction is normal to the ''upper'' surface of Figs. 2(a) and 2(b). The displacements of the atoms on the ith surface layer (with respect to the atomic positions of the ideal surface) are denoted $\delta z(O_i)$ for O and $\delta z(M_i)$ for Sr or Ti; they are positive when pointing outwards, into the vacuum, and negative when oriented inwards, into the bulk. The atomic displacements of the fifth layer atoms (counted from the surface) were found to be smaller than 0.01 Å , which is the numerical limit of the present calculations, and are therefore are not listed in the table. The sixth atomic plane (the center of the slab) was kept frozen during the relaxation due to the symmetry of the supercell and represents the bulk. The average displacement of the ith layer is given as $[\delta z(O_i)+\delta z(M_i)]/2$ and alternates in sign with the first surface layer moving inwards (towards the

TABLE II. Atomic relaxations for the SrO- and the TiO_2-terminated surfaces. The atomic displacements δz are given relative to the ideal surface positions and are positive when pointing towards vacuum, negative when oriented into the bulk. The average displacement of the ith layer is defined as $0.5[\delta z(O_i)+\delta z(M_i)]$, where M_i=Sr or Ti. All results are in units of Å .

	SrO terminated	δz	Average displ.	TiO_2 terminated	δz	Average displ.
1	Sr	−0.26	−0.11	Ti	−0.07	−0.04
	O	+0.04		O	−0.01	
2	Ti	+0.07	+0.04	Sr	+0.18	+0.11
	O	+0.01		O	+0.03	
3	Sr	−0.06	−0.03	Ti	−0.01	0.00
	O	+0.01		O	+0.01	
4	Ti	+0.01	+0.01	Sr	+0.04	+0.03
	O	0.00		O	+0.01	

bulk). Note that we found the largest displacement on the second surface layer of the TiO_2 surface.

The displacements from the ideal lattice positions (Table II) are translated into rumpling parameter r and the change in interlayer spacing d_{ij} in Table III. Like the average displacement, the rumpling parameter is positive for the first layer and alternates in sign when going from the surface into bulk. The oscillating sign of r results from minimizing the electrostatic energy of the surface dipoles that are formed by the relaxation: aligned dipoles with alternating directions have lower energy than any other arrangement.

For comparison, Table III shows rumpling parameters from other theoretical and experimental studies. It is worth pointing out that all *experimental* results were obtained under the assumption that only the first surface layer has nonzero rumpling; such an assumption may have been convenient for fitting experimental data to a model structure but is not necessarily realistic. Both theoretical and experimental studies agree on the positive sign of rumpling of the first surface layer, on both types of surfaces. All sources agree on the oscillating sign of the rumpling parameter.

Also listed in Table III—whenever available—are the relative changes in the interlayer distance; we define the latter as the difference in z coordinates of the *metallic* atoms, in the nearest-neighbor layers, so that $\Delta d_{ij}=\delta z(M_i)$-$\delta z(M_j)$. As the scattering strength of O is much smaller than that of Sr or Ti, the Δd_{ij} are better suited for comparison with experimental data than the average layer displacements given in Table II. We note that the data on $\Delta d_{ij}/d_0$ are not consistent between different experiments; sometimes not even the sign is certain. In contrast, all theoretical results, including those based on phenomenological models, are coherent, both in sign and approximate magnitudes; in particular, there is a very good agreement between our results and similar calculations by Padilla and Vanderbilt.[3] We checked that the remaining differences between the two *ab initio* calculations

TABLE III. Rumpling parameters r (in Å) and percentage changes in the interlayer spacing d_{ij} between the successive layers, from the present calculations (Table II) and from previous studies of the relaxed SrO- and TiO_2-terminated surfaces. The rumpling parameter of the ith layer is defined as $r\equiv\delta z(O_i)-\delta z(M_i)$ and given in Å ; the interlayer distance $d_{ij}\equiv z(M_i)-z(M_j)$ is measured between the *metallic* atoms of the layers i,j and given relative to the ideal interlayer spacing $d_0=a_0/2$; M_i=Sr or Ti.

	Ab initio methods		Shell model		Experiments	
	Present	Ref. 3	Ref. 10	Ref. 6	Ref. 5	Ref. 22
			SrO-terminated surface			
First-layer r	+0.30	+0.22	+0.18	+0.32	+0.16±0.08	+0.16
$\Delta d_{12}/d_0$ (%)	−16.8	−13.8	−9.5	−18.5	−10±2	+5.1
Second-layer r	−0.06	−0.05	–	−0.03	–	–
$\Delta d_{23}/d_0$ (%)	+6.9	+4.8	+2.9	+6.0	+4±2	+2.6
Third-layer r	+0.07	+0.04	–	+0.06	–	–
$\Delta d_{34}/d_0$ (%)	−3.9	–	–	−8.7	–	–
Fourth-layer r	−0.01	–	–	−0.01	–	–
			TiO_2-terminated surface			
First-layer r	+0.07	+0.07	+0.05	+0.05	+0.08±0.08	+0.10
$\Delta d_{12}/d_0$ (%)	−12.8	−11.8	−7.9	−8.0	+2±2	+3.6
Second-layer r	−0.15	−0.12	–	−0.14	–	–
$\Delta d_{23}/d_0$ (%)	+9.4	+6.4	+2.4	+8.1	−2±2	+2.6
Third-layer r	+0.016	+0.01	–	+0.01	–	–
$\Delta d_{34}/d_0$ (%)	−2.2	–	–	−2.2	–	–
Fourth-layer r	−0.026	–	–	−0.02	–	–

TABLE IV. Average surface energy, relaxation energy, and the surface-layer desorption energy calculated for the relaxed SrO- and TiO_2-terminated surfaces using Eqs. (1)–(3). All energies are in units of eV per (1×1) surface area.

E^{PW}	Surface	Surface energy	Relaxation energy		Desorption energy of the surface layer
500 eV	SrO-terminated	average:	−0.30	average:	13.4
500 eV	TiO_2-terminated	1.21	−0.14	−0.22	26.0
500 eV	Asymm. slab calcul.	1.19	−0.21		–
600 eV	Asymm. slab calcul.	1.20	−0.20		–

are not caused by the ''thinner'' slabs used in Ref. 3 but are due to employing different pseudopotentials (the ''ultrasoft'' pseudopotentials[23] in Ref. 3 and the ''optimized'' ones[16] in the present work, while both calculations use the same LDA and plane-wave basis).

IV. SURFACE ENERGY

According to the conventional definition, the surface energy relates to the cleavage energy, i.e, the energy required to cleave the bulk structure and to form two surfaces. When cutting $SrTiO_3$ by a (001) plane, both a SrO- and a TiO_2-terminated (001) surface will appear. As a consequence, one can only speak of an *average* surface energy (equal to half the cleavage energy) but not of the individual SrO or TiO_2 surface energy. The (average) surface energy E_{surf} per (1×1) surface area can be calculated in terms of the energies E^{tot} of the slabs shown in Figs. 2(a) and 2(b):

$$E_{surf}=(1/4)[E_{tot}(\text{symm. SrO-terminated slab}) + E_{tot}(\text{symm. } TiO_2\text{-terminated slab}) - (11/7)E_{tot}(\text{bulk})]. \quad (1)$$

Here E_{tot}(bulk) is calculated on a similar supercell (not shown in Fig. 2), but without the vacuum, and it is understood that all E^{tot} in Eq. (1) are per translational unit cell (supercell). We count that the two symmetric slabs contain altogether four surfaces (two of each type), 11 formula units of $SrTiO_3$, and the supercell we used for calculating the bulk energy comprises of seven formula units. In order to minimize the systematic errors in calculating the energies E_{tot}, we used for all three calculations in Eq. (1) the same supercell, k-point set, and plane-wave cutoff. The resulting (average) surface energy (Table IV) is 1.21 eV per (1×1) surface area, which compares well with the 1.26 eV found in Ref. 3. The surface energy of $SrTiO_3$ (001)—when measured per 1×1 area (i.e., scaled with a_0^2)—is very close to the $BaTiO_3$(001) surface. For the latter linearized augmented PW (LAPW) calculation[24] gave 1.27, and a plane-wave calculation[25] 1.241 eV/(1×1).

All calculated surface energies correspond to *fully relaxed* surfaces. The relaxation part of the surface energy, unlike the surface energy itself, *can* be considered for the two types of surfaces separately. For the SrO-terminated surface we obtained a relaxation energy of −0.30 eV per (1×1) surface area and for the TiO_2-terminated one −0.14 eV; in average, this is −0.22 eV/(1×1), or about 18% of the surface energy. This result compares well with the calculations by Padilla and Vanderbilt,[3] who obtained for the average relaxation energy −0.18 eV.

In addition to symmetric slabs, we also carried out calculations on the asymmetric slab shown in Fig. 2(c). Since both types of surfaces are present in the same supercell, the determination of the (average) surface energy requires one less calculation when the asymmetric slab is used:

$$E_{surf}=1/2[E_{tot}(\text{asymm. slab})-(5/7)E_{tot}(\text{bulk})], \quad (2)$$

but certain precautions have to be taken, which will be discussed in Sec. VI. In such a calculation we obtained an average surface energy of 1.19 eV/(1×1), i.e., less than 2% difference compared to the result from Eq. (1). Also the atomic relaxations and the average relaxation energy [−0.21 eV/(1×1), i.e., ≈5% difference] differ very little from the symmetric slabs, i.e., within the limit of the accuracy of the present calculations (see Sec. VI). With a larger basis set (using cutoff $E^{PW}=600$ eV and the corresponding lattice constant), the surface and relaxation energies (in the asymmetric slab) become 1.20 eV and −0.20 eV, respectively. Thus the uncertainty can be estimated to be ≈0.01 eV/(1×1), in both calculations using Eq. (1) or (2).

In addition to the surface energy, we have also calculated the energy required for removing the atoms of the first surface layer to an infinite distance from the surface (and from one another), i.e., assuming that they become isolated atoms. This is the desorption energy E_{des} of the surface layer. Obviously, this quantity *can* distinguish between the two types of the surface, and, e.g., the desorption energy of the SrO-surface layer, E_{des}(SrO layer) per (1×1) surface area is given by

$$E_{des}(\text{SrO layer})=E_{tot}(\text{symm. SrO-terminated slab}) - E_{tot}(\text{asymm. slab}) - E_{tot}(\text{Sr atom}) - E_{tot}(\text{O atom}) \quad (3)$$

and similarly for the TiO_2 layer. Here the total energy of the isolated (pseudo-) atoms was calculated in the same plane-wave basis, using the same pseudopotentials in an fcc structure with lattice constant 15 Å . The desorption energy of the SrO layer is approximately half that of TiO_2, viz., 13.4 eV versus 26.0 eV (see Table IV). Since the negative of the desorption energy is the *adsorption energy*, we conclude that twice as much energy is gained when Ti, O, and O atoms are adsorbed on the SrO surface than when Sr and O atoms are adsorbed on the TiO_2 surface. When we adopt an alternative

assumption, viz., that the desorbed oxygens form O_2 molecules, the desorbed Sr and Ti atoms condense into the solid phase, and the desorption (adsorption) energies become 9.1 eV (SrO) and 16.0 eV (TiO_2). [The results from Eq. (3) are modified by subtracting the respective cohesion energies.[26,27]]

For the sake of simplicity, we performed this calculation accounting for ideal (unrelaxed) surfaces. Nevertheless, we have seen that the relaxation energies are much smaller than the differences between the above two results, so it should not be much affected.[28] On the other hand, the ratio (or the energy difference) depends on the ''destination'' of the desorbed atoms (or on the ''origin'' of the adsorbed ones)—i.e., on their chemical potential—in contrast to the (average) surface energy (1) that is an intrinsic quantity.

We conclude that taking off the TiO_2 surface layer and uncovering the SrO-terminated surface requires considerably more energy than stripping the SrO layer and creating the TiO_2-terminated surface. Therefore this surface energetics confirms (and quantifies) the earlier experiments suggesting the TiO_2 surface to be more stable than SrO.[9]

V. LONGITUDINAL SURFACE DIPOLE MOMENTS

As already mentioned, relaxation of a surface consisting of both cations and anions can give rise to surface ferroelectricity. In this section, we investigate the *longitudinal* surface dipole moment of the SrO-terminated and TiO_2-terminated surfaces that is caused by relaxation. We are interested in the dipole oriented along the z direction, i.e., perpendicular to the surface, and we will obtain the relevant information by analyzing the longitudinal variation of the electrostatic potentials, microscopic and macroscopic ones, that we obtained in the self-consistent calculations of Sec. III.

The xy-averaged electrostatic potentials $\overline{V}_{es}(z)$, for any of the slab systems in Fig. 2, is defined as

$$\overline{V}_{es}(z)=(1/a_0^2)\int [V_H(x,y,z)+V_{ion}(x,y,z)]dxdy, \quad (4)$$

where V_H is the Hartree potential of the self-consistent calculation, V_{ion} is the electron-ion (pseudo-) potential, and the integral (the plane-averaging) runs over the x and y dimensions of the translational unit cell (area a_0^2). At this point, if we substitute for ionic pseudopotentials their asymptotic form Q/r valid at large distances r from the core, the plane averaging can be performed analytically. We will have

$$V_{ion}(x,y,z)\approx\frac{1}{4\pi\epsilon_0}\sum_\alpha \frac{Q_\alpha}{(x-x_\alpha)^2+(y-y_\alpha)^2+(z-z_\alpha)^2}, \quad (5)$$

where Q_α is the core charge of the atom α at $\vec{r}_\alpha$, and the summation is over all ions of the supercell. Consequences of this approximation will be discussed later in this section.

Replacing V_H by $n(x,y,z)$ [which is related to $V_H(x,y,z)$ by Poisson's equation] and performing the xy averaging, we obtain

$$\overline{V}_{es}(z)=(-1/2\epsilon_0)\left[\int e\overline{n}(z')|z-z'|dz'+\sum_\alpha \frac{Q_\alpha}{a_0^2}|z-z_\alpha|\right], \quad (6)$$

where

$$\overline{n}(z)=(1/a_0^2)\int n(x,y,z)dxdy \quad (7)$$

is the plane-averaged charge density obtained in the self-consistent calculation. The integral in Eq. (6) extends over the supercell of Fig. 2 in the z direction, i.e., along the surface normal, and the core charge Q_α takes values 10, 4, and 6 for the Sr, Ti, and O atoms, respectively. Although Eq. (6) expresses no different physics than Eq. (4), the formula (6) has the advantage of dealing with slabs as with a one-dimensional problem.[29]

$\overline{V}_{es}(z)$ and $\overline{n}(z)$ can be further processed to obtain the *macroscopically* averaged quantities

$$\bar{\bar{V}}_{es}(z)=(1/a_0)\int_{z-0.5a_0}^{z+0.5a_0}\overline{V}_{es}(z')dz', \quad (8)$$

and similarly for $\bar{\bar{n}}(z)$. In Fig. 3 we show the plane-averaged electrostatic potential $\overline{V}_{es}(z)$ and the macroscopically averaged potential $\bar{\bar{V}}_{es}(z)$ for the symmetric SrO-terminated slabs of Fig. 2(a)—the ideal and the relaxed slabs—and similarly in Fig. 4 for the supercell of Fig. 2(b) with the TiO_2-terminated surfaces. All the ''inverted parabola'' potentials in $\overline{V}_{es}(z)$ are the screened Coulomb potentials of the individual ions, and the variation becomes macroscopically smooth in the macroscopic $\bar{\bar{V}}_{es}(z)$: this quantity stays flat inside the slab, as well as in the vacuum, exactly as one expects; the small variations apparent on the relaxed slabs are effect of relaxation.

The value of $\bar{\bar{V}}_{es}(z)$ in the vacuum is taken as zero, and the macroscopic potential inside the slab is then at level $-\Delta V_{es}$. The existence of the potential difference goes along with creation of the surface and formation of a *surface dipole layer*, as the electrons near the surface spill out into the vacuum. The redistribution that reduces their kinetic energy and lowers the total energy of the surface system.[30] The potential difference ΔV_{es} thus can be used for reading the surface dipole moment. Reasoning in analogy with the potential variation across the capacitor, we find that the surface dipole moment per (1×1) surface area can be obtained by multiplying ΔV_{es} by the (1×1) area of the surface, i.e., by a_0^2. Technically, we take the potential difference $-\Delta V_{es}$ between the $\bar{\bar{V}}_{es}(z)$ in the middle of the vacuum and on the center of the slab, and it is then understood that both the outermost surface plane and several subsurface layers of the slab contribute to the ''surface dipole.'' From the values of ΔV_{es} corresponding to the ideal and relaxed surfaces we then determine the *change* in ΔV_{es} caused by relaxation, i.e., the *relaxation-induced* surface dipole moment. These values read from Figs. 3 and 4, and the corresponding surface dipoles calculated from them are listed in Table V, for both ideal and relaxed SrO- and TiO_2-terminated surfaces.

It is worth pointing out that V_{es}, $\overline{V}_{es}(z)$, and $\bar{\bar{V}}_{es}(z)$ obtained by using the substitution (5) are only exact at large

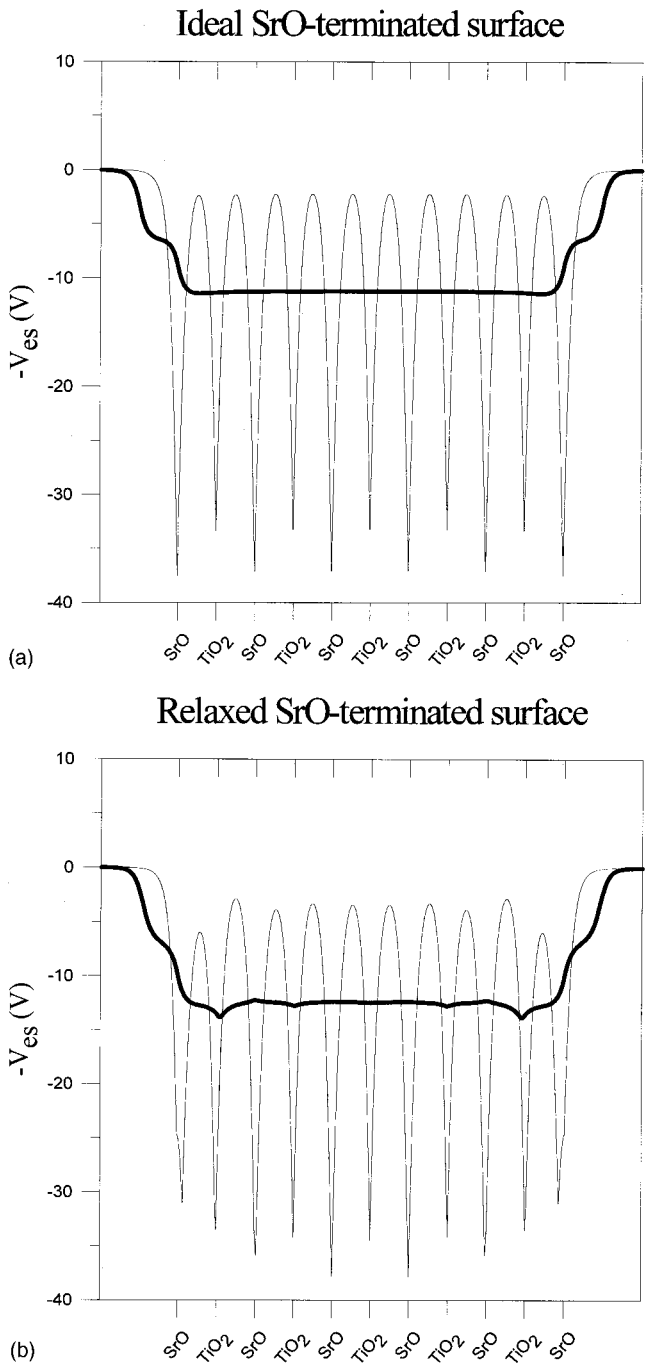

FIG. 3. The xy-averaged (plane-averaged) electrostatic potential $\overline{V}_{es}(z)$, Eq. (6), of the SrO-terminated slab, Fig. 2(a), and $\bar{\bar{V}}_{es}(z)$ (heavy lines), the macroscopically averaged $\overline{V}_{es}(z)$, Eq. (8). (a) Ideal SrO-terminated surface; (b) relaxed surface.

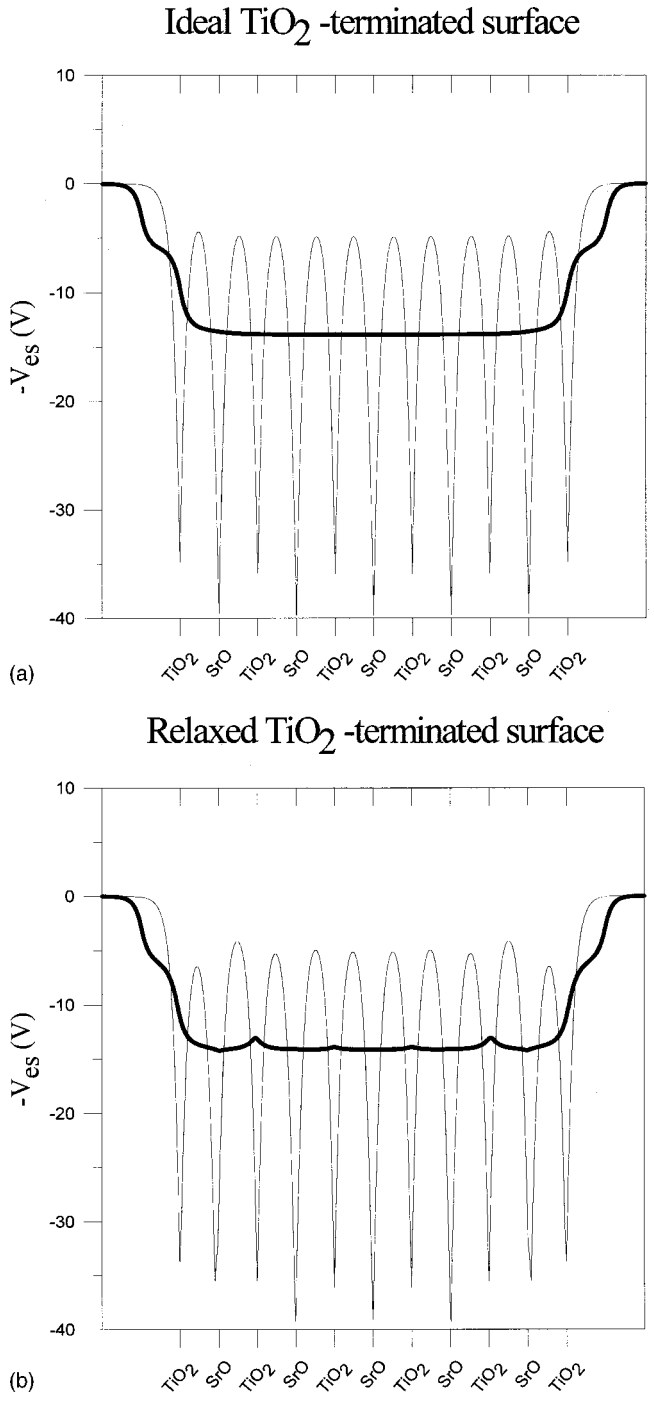

FIG. 4. As Fig. 3, but for the TiO_2-terminated surface.

distances from the cores—i.e., in the vacuum region. In the vicinity of the cores—i.e., inside the slab—our averaged V_{es} are only approximate, and the error induced by Eq. (5) could be evaluated by (numerically) integrating the difference between the actual pseudopotential $v_\alpha(r)$ and the approximation Q_α/r. Although ΔV_{es} are only approximate values, we obtain the relaxation-induced change in ΔV_{es} accurately, because both calculations contain the same error in determining ΔV_{es} that refers to $\bar{\bar{V}}_{es}(z)$ at the (fixed) center of the slab.

The *relaxation-induced* surface dipole moment is much stronger on the SrO- than on the TiO_2-terminated surface—although the surface dipole moment itself is of comparable magnitude for both surfaces, whether relaxed or ideal ones. The relaxations on both surfaces tend to *increase* the surface dipole layers (Table V) with negative dipole moments pointing *inwards*, into the bulk.

In order to compare the polarization induced by relaxation in $SrTiO_3$ with that caused by the ferroelectric distortion in $BaTiO_3$, we ascribe the dipoles 0.11 and 0.02 of Table V to the volume a_0^3, i.e., to the surface layer of thickness a_0. This yields 2.85 and 0.52×10^{-6} C/cm^2 for polarization of the respective SrO and TiO_2 surface layers, values that can be compared with the polarization of the bulk $BaTiO_3$ of 26 $\times10^{-6}$ C/cm^2 (Ref. 31). Thus the relaxation-induced (sur-

TABLE V. The surface dipole moment of the 1×1 surface area of the ideal and relaxed SrO- and TiO_2-terminated surfaces, as calculated from the variation of the macroscopic potential $\bar{\bar{V}}_{es}(z)$ shown in Figs. 3 and 4. For comparison with previous publications, the entries $q_i r_i$ give the relaxation-induced dipole moments evaluated naively as a product of the rumpling parameter of the ith layer (Table III) and of the *valence* charges (+2, +4, and −2 for Sr, Ti, and O, respectively); they correspond to including the first layer only $(-q_1 r_1)$, or all four relaxed layers $(-\Sigma_{i=1}^{i=4} q_i r_i)$.

	SrO-terminated	TiO_2-terminated
	Present calculation	
Ideal surface	$-0.96\ e$ Å	$-1.19\ e$ Å
Relaxed surface	$-1.07\ e$ Å	$-1.21\ e$ Å
(relaxed surface)	$-0.11\ e$ Å	$-0.02\ e$ Å
-(ideal surface)	-1.76×10^{-28} C cm	-0.32×10^{-28} C cm
$-q_1 r_1$	$-0.60e$ Å $(q_1=2)$	$-0.28e$ Å $(q_1=4)$
$-\Sigma_{i=1}^{i=4} q_i r_i$	$-0.46\ e$ Å	$+0.01\ e$ Å
	Reference 6	
Shell model	$-0.45\ e$ Å	$-0.17\ e$ Å
	Reference 5	
Expt. $(-q_1 r_1)$	$-0.32\ e$ Å	$-0.32\ e$ Å

face) polarization amounts only to 11% and 2% of the $BaTiO_3$ bulk polarization for the two surfaces—values that are not large but certainly not negligible.

Table V includes relaxation-induced dipole moments derived in the previous shell model[6] and experimental[5] studies. The moments in Ref. 5 were obtained by only allowing first-layer rumpling and assuming the valence charges (4 for Ti, 2 for Sr, and −2 for O). From our present results we can make the same simple estimate, using the data from Table III. This allows us to distinguish between the dipole moments induced by the relaxation of only the first surface layer $(-q_1 r_1)$ and those of all four surface layers $(-\Sigma_{i=1}^{i=4} q_i r_i)$. The large difference between these two results (Table V) demonstrates that the relaxation effects do not originate only from the first surface layer. The fact that the dipole moments as products of the type $q_i r_i$ are very different from those obtained with ΔV_{es} demonstrates that the systems studied here are far from ideal ionic systems; as a matter of fact, instead of using ionic charges, we should use *effective* charges—a notion well known in the context of lattice dynamics.

The shell-model study[6] is more realistic since it calculates the relaxation-induced dipole moments from the displacements of ion cores, the shells, and the core and shell charges, which amounts to modeling the *charge relaxation*. Effects of surface rumpling were taken into account down to the sixth surface layer, and, although the displacements of the ion cores of the relaxed structures are fairly similar to what we obtained here (Table III), the dipole moments are not. This clearly points to an inadequate description of polarization by simple mechanical models.

VI. PARTICULARITIES OF THE CALCULATIONS WITH THE ASYMMETRIC SLAB

The symmetric slabs [Figs. 2(a) and 2(b)] that have been used for most of the calculations in Secs. III–V have the advantage of guaranteeing that neither the construction of the slab nor the periodic boundary conditions introduce any spurious electric fields that might invalidate the calculations, or that would require a special treatment. Nevertheless, in some cases an asymmetric slab of the type Fig. 2(c) can be used, provided one understands the electric fields in the system and takes appropriate correction measures. In Secs. III and IV, we found the unexpected result that the relaxed structures, surface energy and the average relaxation energy, are different very little between symmetric or asymmetric slabs, although only the former with a mirror plane [Figs. 2(a) and 2(b)] should lead to meaningful results. Qualitatively, it is easy to see the origin of these surprisingly small differences: the surface dipole moments are of comparable magnitude for both surfaces. In this section we will discuss, for the example of the slab in Fig. 2(c), under which conditions the asymmetric slabs can be used to investigate surface systems.

The key quantity here is the macroscopic electric field and its variation across the supercell. In Fig. 5 we show the microscopic and macroscopic electrostatic potentials $\overline{V}_{es}(z)$ and $\bar{\bar{V}}_{es}(z)$, which one obtains for the ideal (unrelaxed) asymmetric slab [Fig. 2(c)] when the boundary conditions are properly taken into account. One sees a small slope in the vacuum region (and an even smaller within the slab), in contrast to Figs. 3 and 4 (with zero slope). Thus there is a nonzero macroscopic electric field in the supercell (Fig. 5). This field is a consequence of the artificial periodic repetition of the (+/− charged) asymmetric slab.

Schematically, a solid with two different surfaces can be represented by the (macroscopic) electrostatic potential in Fig. 6(a): this sketch corresponds to an (infinite) slab occurring *alone*, in free space.[32] The most important feature of this diagram is in the two different steps ΔV_{es}, implying that the corresponding dipole layers on the two surfaces are different. This can be represented by a small surface charge,[30] positive on the left side, negative on the right one. However, this violates the periodic boundary conditions, since potentials are different on the two sides by $\delta(\Delta V_{es}) \equiv \Delta V_{es} - \Delta V'_{es}$. In order to obtain the potential variation in the system of repeated slabs [bottom of Fig. 6(b)] the Poisson equation must be solved anew, with the appropriate boundary conditions. There is nevertheless an equivalent (and standard) way of constructing such a potential, namely by starting from the variation sketched in Fig. 6(a) and superimposing the *depolarizing field*

$$E_{depol} \equiv -\delta(\Delta V_{es})/(d_1+d_2) \tag{9}$$

or

$$V_{depol}(z) \equiv \delta(\Delta V_{es}) z/(d_1+d_2). \tag{10}$$

The $V_{depol}(z)$ cancels the difference in ΔV_{es} (i.e., the effect of the surface charges) at the supercell boundaries so that the periodic boundary condition

$$\overline{f}(z) = \overline{f}(z+d_1+d_2) \tag{11}$$

is satisfied. The potential (10) is sketched in Fig. 6(b) by the broken line, and the resulting potential of the ''linear chain'' of slabs and vacua is shown as well. It is this scheme that we will use for interpretation of the behavior of the potentials in Fig. 5.

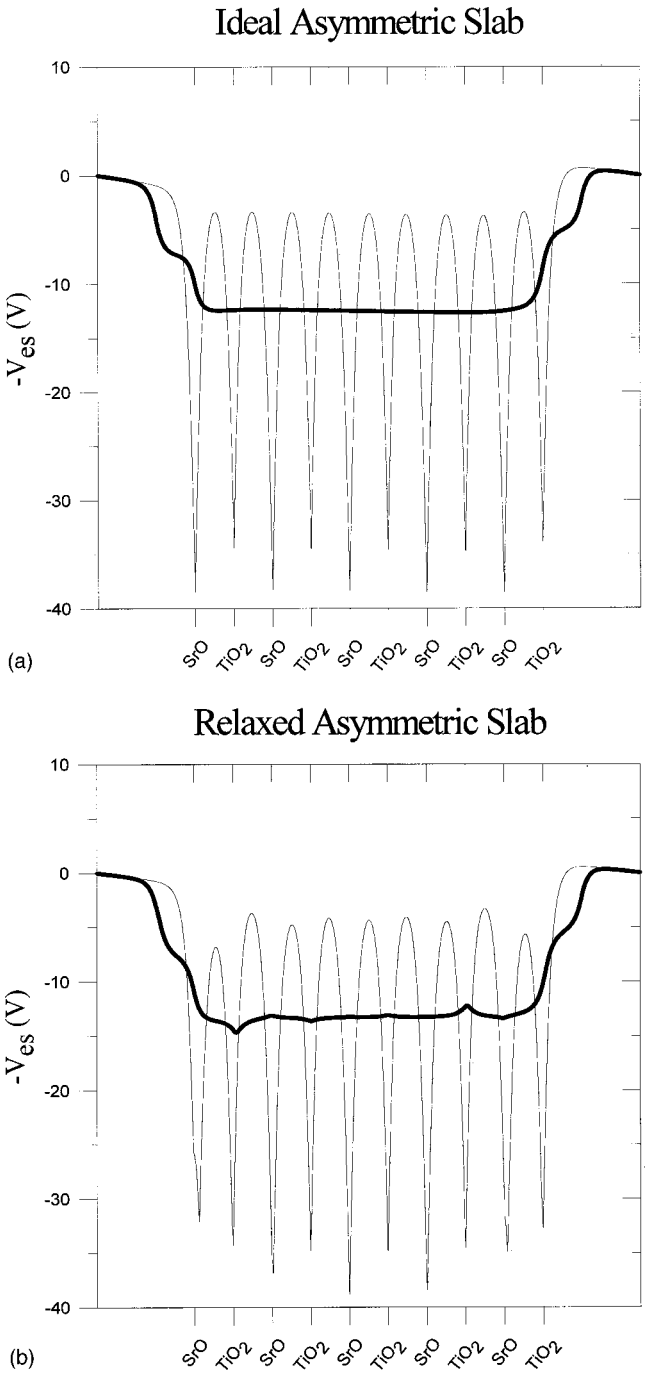

FIG. 5. As Fig. 3, but for the ideal asymmetric slab.

Due to screening, the electric field inside the slab is much weaker than in vacuum (Fig. 5), and the ratio of the two slopes is given by the dielectric constant of the slab. In the calculations shown in Fig. 5(a) we can estimate the corresponding slopes of 0.263 and 0.037 V/Å , and their ratio ≈ 7 should be compared to $\epsilon = 5.36$–7.01,[33] the static dielectric constant of bulk $SrTiO_3$. This is a good agreement, considering that large errors were induced by estimating the slopes from the graph in Fig. 5.

Similar calculations with the depolarizing field have already been performed in Ref. 24 on asymmetric slabs of $BaTiO_3$. Due to the strong polarization already present in the bulk, the depolarizing fields are very strong and thus cause large deviations from results obtained on the symmetric

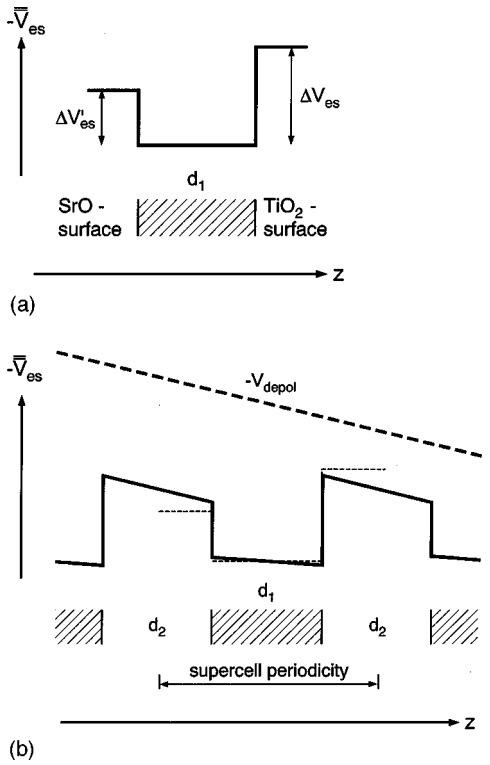

FIG. 6. Schematic representation of the electrostatic potential $-\bar{V}_{es}(z)$, Eq. (8), for a layer of $SrTiO_3$. (a) Isolated single slab in free space. (b) The same slab, periodically repeated. As a consequence of the boundary conditions, a macroscopic field appears in the system [depolarizing field, Eq. (10)].

slabs. In $SrTiO_3$, however, only moderate polarization occurs and thus V_{depol} is weak, so that the (average) surface energy is affected only by 0.02 eV/(1×1). This weakness of the electric field inside the slab (0.037 V/Å) explains also why the detailed geometries of the relaxed structures were found to be very similar for the symmetric and asymmetric slabs. Using the valence charges $+2$, $+4$, and -2 on Sr, Ti, and O we can estimate that the ''additional'' forces on atoms originating from the E_{depol} will be, e.g., 0.07 eV/Å (on Sr), which is not much larger than the value at which we stopped relaxing. This means that in situations with similar values of $\delta(\Delta V_{es})$, d_1, d_2, and ϵ, the relaxations *may be* obtained from asymmetric supercells [Fig. 2(c)] and are comparable to results obtained with a less stringent relaxation criterion.

Analogously we can estimate the effect on energies. The main difference in the results from the symmetric and asymmetric slab calculations comes from the depolarizing field in the vacuum region. The energy of electric field in vacuum is given by $(\epsilon_0/2)\int E^2 dV$. Taking the integral over the volume a_0^3 of the vacuum region and assuming a constant electric field, we can estimate an additional 0.01 eV per (1×1) surface area in the surface energy. This is precisely the order of magnitude of the difference in surface energies that we obtained from the calculations on the two types of slabs (Table IV).

Calculations using the asymmetric slab have the advantage of dealing with both surfaces simultaneously. This may not necessarily mean less numerical effort, e.g., in obtaining the structural relaxations, but the results on a slab *without* a symmetry plane enable certain reasonings that otherwise

would not be possible, as, e.g., those concerning the desorption/adsorption energies in Sec. IV.

We can conclude from these examples that, in future studies of similar systems with two different types of surfaces (and without a permanent polarization in the bulk), the asymmetric slabs *can* provide realistic results on surface relaxations and surface energies, provided that the slab systems are sufficiently thick (d_1+d_2) and do not exhibit too large surface charges $[\delta(\Delta V_{es})]$, and that their dielectric constant ϵ is not too small. In the system studied in this work we find the effects of the depolarizing electric field weak enough to obtain *numerically* correct relaxed structures and surface and desorption energies—even if, strictly speaking, only the results obtained on the symmetric cells, without any macroscopic electric field inside the slab, are physically meaningful.

VII. CONCLUSIONS

We've carried out an *ab initio* study of the SrO- and TiO_2-terminated surfaces of $SrTiO_3$. The relaxed structures, the surface energy, and the individual relaxation energies were determined. The comparison of the surface-layer desorption energy for the two types of surfaces explains why the TiO_2-terminated surface appears to be more stable, as found experimentally. The longitudinal surface dipole moments caused by the relaxation are found to be small on both surfaces but not negligible. It turns out that the largest contribution to the surface polarization does not always come from the first surface layer (as has been assumed in previous semiempirical models and in the experimental data analyses), and that the surfaces in question are far from being ideal ionic systems: the electronic charge relaxation cannot be neglected. Finally, the analysis and understanding of the macroscopic electrostatic potential in the case of asymmetric slabs explain why the latter can provide numerically correct results.

ACKNOWLEDGMENTS

We are grateful to G. Chern for having suggested this study. We want to acknowledge useful discussions with E. Tosatti, D. Vanderbilt, Y.T. Lu, and A. Postnikov, and we thank K. Schwarz for a critical reading of the manuscript. This work was supported by the National Science Council in Taiwan (ROC) and the CNRS (Centre National de la Recherche Scientifique) in France. The computer resources were partly provided by the National Center for High-Performance Computing in HsinChu, Taiwan.

*Email: ccheng@ibm7a.phy.ncku.edu.tw
†Email: kunc@ccr.jussieu.fr
‡Email: mhslee@mail.tku.edu.tw

[1] P. Chaudhari, R.J. Gambino, R.H. Koch, R.B. Laibowitz, and T.R. Mcguire, Phys. Rev. Lett. **58**, 2684 (1987); T. Terashima, Y. Bando, K. Iijima, K. Yamamoto, K. Hirata, T. Hayashi, K. Kamigaki, and H. Terauchi, *ibid.* **65**, 2684 (1990).
[2] V. Ravikumar, D. Wolf, and V.P. Dravid, Phys. Rev. Lett. **74**, 960 (1995).
[3] J. Padilla and D. Vanderbilt, Surf. Sci. **418**, 64 (1998).
[4] Z.-Q. Li, J.-L. Zhu, C. Q. Wu, Z. Tang, and Y. Kawazoe, Phys. Rev. B **58**, 8075 (1998).
[5] N. Bickel, G. Schmidt, K. Heinz, and K. Multer, Phys. Rev. Lett. **62**, 2009 (1989).
[6] E. Heifets, S. Dorfman, D. Fuks, E. Kotomin, and A. Godon, J. Phys.: Condens. Matter **10**, L347 (1998).
[7] M.E. Lines and A.M. Glass, *Principles and Application of Ferroelectrics and Related Materials* (Clarendon Press, Oxford, 1977).
[8] M. Kawasaki, K. Takahashi, T. Maeda, R. Tauchiya, M. Shinohara, O. Ishiyama, T. Yonezawa, M. Yoshimoto, and H. Koinuma, Science **266**, 1540 (1994).
[9] See, for example, J. Zegenhagen, T. Haage, and Q.D. Jiang, Appl. Phys. A: Mater. Sci. Process. **67**, 711 (1998).
[10] J. Prade, U. Schrodert, W. Kress, F.W. de Wette, and A.D. Kulkarni, J. Phys.: Condens. Matter **5**, 1 (1993).
[11] P. Hohenberg and W. Kohn, Phys. Rev. **136**, B864 (1964).
[12] W. Kohn and L.J. Sham, Phys. Rev. **140**, A1133 (1965).
[13] D.M. Ceperley and B.J. Alder, Phys. Rev. Lett. **45**, 566 (1980).
[14] M.C. Payne, M.P. Teter, D.C. Allan, T.A. Arias, and J.D. Joannopoulow, Rev. Mod. Phys. **64**, 1045 (1992).
[15] H.J. Monkhorst and J.D. Pack, Phys. Rev. B **13**, 5188 (1976).
[16] J.S. Lin, A. Qteish, M.C. Payne, and V. Heine, Phys. Rev. B **47**, 4174 (1993).
[17] L. Kleinman and D.M. Bylander, Phys. Rev. Lett. **48**, 1425 (1982).
[18] As a consequence, the nonlinear core correction is not applied.
[19] J. Goniakowski, J.M. Holender, L.N. Kantorovich, and M.J. Gillan, Phys. Rev. B **53**, 957 (1996); K. Refson, R.A. Wogelius, D.G. Fraser, M.C. Payne, M.H. Lee, and V. Milman, *ibid.* **52**, 10 823 (1995).
[20] *Numerical Data and Functional Relations in Science and Technology—Crystal and Solid State Physics*, edited by T. Mitsui and S. Nomura, Landolt-Bornstein, New Series, Group III, (Springer, Berlin, 1982), Vol. 16, Pt. A.
[21] H. Hellmann, *Einführung in die Quantenchemie* (Deuticke, Leipzig, 1937), pp. 61 and 285; R.P. Feynman, Phys. Rev. **56**, 340 (1939).
[22] T. Hikita, T. Hanada, and M. Kudo, Surf. Sci. **187/188**, 377 (1993); T. Hikita, T. Hanada, and M. Kudo, J. Vac. Sci. Technol. A **11**, 2649 (1993).
[23] D. Vanderbilt, Phys. Rev. B **41**, 7892 (1990).
[24] R.E. Cohen, Ferroelectrics **194**, 323 (1997).
[25] J. Padilla and D. Vanderbilt, Phys. Rev. B **56**, 1625 (1997).
[26] Here we used the *experimental* cohesion energies of 1.70 eV/atom, 4.87 eV/atom, and 2.58 eV/atom for Sr, Ti, and O, respectively, taken from Ref. 27.
[27] K.A. Gschneidner, Jr., in *Solid State Physics*, edited by F. Seitz, D. Turnbull, (Academic Press, New York, 1964), Vol. 16, p. 344; P.W. Atkins, *Physical Chemistry*, 4th ed. (Oxford University Press, Oxford, 1990), p. 938.
[28] For the same reason we have not attempted to improve the accuracy of the three atomic calculations involved, which (given the size of the fcc cells) adds to the above results an uncertainty of the order of 1 eV/(1×1) surface area.
[29] Equation (6) might also be preferred to Eq. (4) when self-consistent codes are used that only provide the $n(r)$ or $n(G)$ on output, but do not offer any easy access to the potential V_H.

[30] See, for example, Chap. 18 in N. W. Ashcroft and N. D. Mermin, *Solid State Physics* (Holt-Saunders, New York, 1976).
[31] E.C. Subarao, Ferroelectrics **5**, 267 (1973).
[32] For the sake of simplicity we do not consider that, in the fully general case, the bottom of the potential ''well'' in Fig. 6(a) might be tilted. Nevertheless, in such a case our reasonings would have to be modified very little: only the dielectric constant would be ''visualized'' differently.
[33] *Numerical Data and Functional Relations in Science and Technology*, Landolt–Börnstein New Series, Group III (Springer, Berlin, 1976), Vol. 11, p. 606.